Energy & Environmental Science

PAPER

View Article Online
View Journal | View Issue

Cite this: *Energy Environ. Sci.*, 2014, **7**, 3391

Superadiabaticity in reaction waves as a mechanism for energy concentration

Sayalee G. Mahajan,[a] Joel T. Abrahamson,[ab] Stephanie Birkhimer,[a] Eric Friedman,[ac] Qing Hua Wang,[a] Margaret Beck[d] and Michael S. Strano*[a]

Received 27th February 2014
Accepted 14th July 2014

DOI: 10.1039/c4ee00678j

www.rsc.org/ees

Spatially propagating reaction waves are central to a variety of energy applications, such as high temperature solid phase or combustion synthesis, and thermopower waves. In this paper, we identify and study a previously unreported property of such waves, specifically that they can generate temperatures far in excess of the adiabatic limit. We show that this superadiabaticity occurs when a reaction wave in either one dimension (1D) or two dimensions (2D) impinges upon an adiabatic boundary under specific reaction and heat transfer conditions. This property is studied analytically and computationally for a series of 1D and 2D example systems, producing an estimate of the upper bound for excess temperature rise as high as 1.8 times the adiabatic limit, translating to temperatures approaching 2000 K for some practical materials. We show that superadiabaticity may enable several new types of energy conversion mechanisms, including thermophotovoltaic wave harvesting, which we analyze for efficiency and power density.

Broader context

Heat at low temperatures is one the hardest forms of energy to convert to electrical power. At the same time, it constitutes an abundant and widely distributed form of energy. Thermodynamic limits bracket low temperature energy conversion, but practical conversion technologies also benefit from higher temperature differences in operation. Concepts that allow the spatial concentration and transfer of heat from a higher temperature reservoir can dramatically improve energy conversion. In this work, we identify a new mechanism whereby chemical energy can be converted to heat at temperatures in excess of the adiabatic limit, spatially concentrated into a reacting wavefront. This superadiabaticity occurs when a fuel decomposes or reacts to form a self-propagating reaction wave impinging upon an adiabatic boundary. Under a range of conditions, temperatures in excess of the adiabatic limit can be reached, thus upgrading the value of the energy source to a higher temperature and spatially focusing it at the boundary for more efficient harvesting. This theory motivates several new energy conversion technologies, including a thermophotovoltaic wave system that allows one to operate a fuel reaction using superadiabaticity, generating thermionic emission not otherwise possible for capture using high efficiency photovoltaics. This theory of superadiabaticity has the potential to realize higher efficiency energy conversion technologies in this way.

1. Introduction

In an exothermic reaction, the maximum temperature that can be attained is bounded by the adiabatic reaction limit.[1–3] The adiabatic temperature rise, similar to the adiabatic flame temperature[3] or adiabatic combustion temperature of a system,[4] corresponds to the condition at complete chemical conversion whereby the enthalpy of reaction is translated into sensible heat of the product mixture without phase change. This limiting temperature is an inherent reactant property and determined exclusively by thermodynamics. Reaction temperature, in turn, is central to energy conversion mechanisms for a variety of reasons. It sets the high temperature reservoir for Carnot efficiency *via* the 2nd law of thermodynamics.[5–7] It also determines the relative weighting of thermal energy transport mechanisms with poor efficiency such as conduction against those of high efficiency such as radiation.[8–10] For many energy conversion technologies, such as thermoelectrics,[6,7] thermophotovoltaics,[11–13] and combustion synthesis,[4] performance metrics such as efficiency, power density or final product properties are governed by temperature. In these processes, their overall efficiency increases with increased temperature. Hence, mechanisms that concentrate thermal energy and elevate temperature have utility in such conversion technologies.

Reaction waves feature prominently in the analysis of combustion synthesis or solid phase materials synthesis,[4,14] and more recently as an electrical energy generation mechanism in thermopower waves.[15] Reaction waves exhibiting self-propagation have been previously studied by Zeldovich and Frank-

[a]*Department of Chemical Engineering, Massachusetts Institute of Technology, 77 Massachusetts Ave, Cambridge, MA, USA. E-mail: strano@mit.edu*

[b]*Department of Chemical Engineering and Materials Science, University of Minnesota, Twin Cities, Minneapolis, MN 55455, USA*

[c]*Roxbury Community College, 1234 Columbus Ave, Roxbury Crossing, MA 02120, USA*

[d]*Department of Mathematics and Statistics, Boston University, 111 Cummington Mall, Boston, MA 02215, USA*

Kamenetskii who investigated flame propagation for gaseous mixtures.[16,17] Abrahamson *et al.* studied 1D reaction waves for solid fuels and found an analytical expression for the system temperature.[18] Ji-Huan He performed an analysis to obtain an expression for the condition to obtain oscillatory thermal waves in a non-adiabatic system.[19] Weber *et al.* obtained expressions for temperature profiles of the reaction wavefront for both gaseous and solid fuels.[20] Numerical analysis of the governing heat and mass balance equations was also carried out by Weber *et al.*,[20] Mercer *et al.*[21–23] and Gray *et al.*[17]

In this work, we identify for the first time the property of superadiabaticity that occurs when a reaction wave in either one dimension (1D) or two dimensions (2D) impinges upon an adiabatic boundary under specific but broadly applicable conditions, leading to a temperature rise above the adiabatic limit. Superadiabaticity is shown to enable the concentration of thermal energy, increasing the reaction temperature to up to 1.8 times the adiabatic limit. For example, for an energetic material like nitrocellulose which shows an adiabatic temperature rise of about 1100 K, superadiabatic temperatures up to 2000 K are possible. This superadiabaticity can form the basis of new energy conversion schemes. Thermal radiation is a transfer mechanism more easily captured and efficiently converted than conduction. Increasing the temperature will allow us to effectively harvest an increased amount of energy transported *via* radiation by using high efficiency energy conversion technologies such as photovoltaics. In this work, we propose how a thermophotovoltaic wave system can be used to convert chemical energy to electrical energy with efficiency and power density predicted to increase for superadiabatic conditions.

We begin by reviewing past work in the field of numerical analysis of reaction waves. Then, we demonstrate our new finding of superadiabaticity by numerical analysis of different types of reaction systems. Finally, we demonstrate the operation of a thermophotovoltaic wave system for energy conversion from chemical to electrical energy.

2. Introduction to reaction waves for energy conversion

In this section, we review previous work on reaction waves, specifically their temperature and velocity when propagating at steady state. We discuss results for numerical analysis of 1D reaction waves and 2D reaction wave systems simplified to 1D systems. The equations presented in this section act as a precursor for our analysis of superadiabaticity.

Consider a reaction wave propagating in a 1D incompressible, immobilized medium according to 1st order reaction kinetics without phase change. The corresponding version of Fourier's law that applies is shown in eqn (1):

$$\rho C_p \frac{dT}{dt} = k\frac{\partial^2 T}{\partial x^2} + (-\Delta H)k_0 W e^{-\frac{E_a}{RT}} \quad (1)$$

$$\frac{dW}{dt} = -k_0 W e^{-\frac{E_a}{RT}} \quad (2)$$

In the heat transfer eqn (1), ρ is the density of fuel, C_p is the specific heat capacity of the fuel, T is the temperature, x is the distance coordinate, k is the thermal conductivity of the fuel, $(-\Delta H)$ is the exothermic heat of reaction, k_0 is the first order reaction constant and E_a is the activation energy of the fuel reaction. In the mass transfer eqn (2), W is the mass concentration of the fuel. The Arrhenius form of rate constant is used for the assumed 1st order reaction mechanism for fuel reaction. For solid fuels, the diffusion term in the mass balance equation is ignored. Both of these equations are non-dimensionalized to give the following non-dimensional variables: temperature u, time τ, mass w, and distance ξ.

$$u = \frac{R}{E_a}T,\ \tau = \frac{t(-\Delta H)Rk_0}{C_p E_a} = \frac{tk_0}{\beta},\ w = \frac{W}{\rho},$$
$$\xi = x\left[\left(\frac{\rho C_p}{k}\right)\left(\frac{(-\Delta H)k_0 R}{C_p E_a}\right)\right]^{\frac{1}{2}} \quad (3)$$

The non-dimensional governing equations for heat and mass transfer are eqn (4) and (5):

$$\frac{\partial u}{\partial \tau} = \frac{\partial^2 u}{\partial \xi^2} + we^{-\frac{1}{u}} \quad (4)$$

$$\frac{dw}{d\tau} = -\beta we^{-\frac{1}{u}} \quad (5)$$

While the adiabatic temperature rise for a reaction accounts for the specific heat capacity of the reaction mixture, traditional numerical analysis of self-propagating reaction waves analyzing systems based on solid fuel define the adiabatic temperature rise as $1/\beta$ which depends only on the reacting solid fuel's properties.[18,23,24]

Hence, the inverse non-dimensional adiabatic temperature rise in the system after the fuel has completely reacted is represented by β [18] where $(-\Delta H)/C_p$ is the dimensional adiabatic temperature rise.

$$\beta = \frac{C_p E_a}{(-\Delta H)R} \quad (6)$$

We exclude the case of a phase change as the reaction proceeds from reactants to products. The adiabatic temperature rise can be either found experimentally by using a calorimeter or calculated analytically by assuming an exothermic reaction and its products. Values of the adiabatic temperature rise for various fuels have been calculated by Hada *et al.*[2]

Abrahamson *et al.* performed a numerical analysis of this system of equations for 1D self-propagating waves for solid fuels by using COMSOL, a finite element method software for partial differential equations.[24] An analytical expression for the reaction wave temperature profile, u_{ana}, was found using a logistic function.[18,24] We make use of this expression when studying superadiabaticity in an adiabatic batch reactor system.

$$u_{\text{ana}} = \frac{1/\beta}{\left(1 + Q\mathrm{e}^{cQ(\xi - c\tau)}\right)^{1/Q}} \tag{7}$$

In eqn (7), c is the constant reaction wavefront velocity. Here, $Q = f(\beta)$ is a system property and is related to the curvature of the temperature profile near the asymptotes and informs the wave symmetry at the reaction front. This analytical expression for the steady wave, u_{ana}, was used with the non-dimensional form of the equations along with Dirichlet boundary conditions to obtain an expression for the wave velocity c:

$$c = \mathrm{e}^{-\left(\frac{\beta}{2}\right)(1+Q)^{1/Q}} \sqrt{\frac{\beta}{Q}\left[-1 + (1+Q)^{\frac{(1+Q)}{Q}}\right]} \tag{8}$$

Also, an expression for $Q(\beta)$ was obtained by empirical analysis.

$$Q = 0.0061\beta^3 - 0.077\beta^2 + 1.2531\beta - 0.208 \tag{9}$$

Choi *et al.* introduced the experimental realization of the concept of thermopower waves to convert chemical energy to electrical energy using self-propagating chemical reaction waves.[15] While that work mainly focused on multi-walled carbon nanotubes as thermal conduits, there have been other advances in the field of thermopower waves. As described in a recent review paper on thermopower waves,[25] apart from multi-walled carbon nanotubes, other conduits such as single-walled carbon nanotubes,[26,27] ZnO,[28] Bi_2Te_3 on alumina and terracotta,[29] Sb_2Te_3 on alumina and terracotta,[30] MnO_2 on alumina[31] and Sb_2Te_3 on carbon nanotubes[32] have also been tested for launching thermopower waves. All these systems have a common feature of self-propagating reaction waves launched on thermal conduits with specific thermal and electrical properties, and all such waves can be theoretically described by simplified system of equations given by eqn (4) and (5).

Recently, Ji-Huan He performed analysis on various systems of equations that model soliton waves,[19] which are the solution to non-linear partial differential equations that give rise to non-diffusive waves.[19] The analysis carried out by Abrahamson *et al.* is one example of a soliton wave. The non-diffusive nature of such reaction waves is the cause of adiabatic temperature rise being maintained in the region behind the reaction wavefront. Ji-Huan He performed an analysis of modified system of equations by accounting for heat loss from the thermal wave as it moves ahead and found the condition that gives rise to oscillatory waves.[19]

Weber *et al.* performed an asymptotic analysis of a system of equations for a 1D system accounting for heat loss in systems containing gaseous and solid fuels. They derived expressions for temperature in the region far away ahead of and behind the wavefront as a function of position and time.[20] Similarly, expressions predicting wave velocity were found to be dependent only on the value of β for both gaseous and solid fuels.

Numerical and asymptotic analyses have also been performed for 2D reaction waves. Work by Mercer *et al.* studied a generalized system of equations representative of a 1st order reaction occurring in a 2D system.[21] To study these dependent partial differential equations, a numerical analysis was carried out by a conventional finite difference scheme for the spatial coordinates and an Euler scheme for the time variable. Numerical analysis was also carried out by reducing the 2D model to a 1D model by using 'center-manifold analysis'. Results obtained from both methods of analyses support the existence of self-propagating reaction waves in 2D. The wave velocity analyzed using both these approaches *i.e.* numerical analysis and center-manifold analysis showed good agreement.[21] Mercer *et al.*[22,23] and Gray *et al.*[17] have also performed numerical analysis on a system of self-propagating exothermic reaction waves.

In this paper, we study such reaction waves when impeded by an adiabatic boundary. Under certain system conditions, our numerical results show the system temperature rising beyond the adiabatic temperature for both 1D and 2D reaction waves. We have formulated an analytical expression that shows superadiabaticity to be a function of the thermochemical properties of the fuel and wave heat transfer properties. We conclude by performing calculations to show how superadiabaticity can be used to establish a new thermophotovoltaic wave system which can operate at higher energy conversion efficiency because of the improved focusing of heat energy by superadiabaticity.

3. Numerical analysis of superadiabatic temperatures shown by various fuel configurations with an adiabatic boundary

A self-propagating reaction wave system can be visualized and studied in a variety of fuel and system configurations. We begin our study of superadiabaticity in reaction waves by considering a simple system of a single batch reactor being initiated by a 1D reaction wave.[18] This is followed by studying increasingly complex reaction wave systems such as multiple batch reactors in series, a 1D layer of fuel and a 2D fuel layer, each with a simple Gaussian heat input and an adiabatic boundary.

3.1. Superadiabaticity in a batch reactor with an adiabatic boundary and an incoming 1D reaction wave initiation

Consider a region of fuel in a layer, equivalent to a single batch reactor being surrounded by an adiabatic boundary. Fig. 1a shows a schematic of such a system. On one side of the reactor, it is exposed to a self-propagating reaction wave that acts as a source of ignition. The other side of the reactor is an adiabatic boundary. The reactor can only exchange heat with the incoming wave and not with any region of its surrounding atmosphere.

The temperature of this fuel is governed by the energy balance eqn (10).

$$mC_{\text{p}}\frac{\mathrm{d}T}{\mathrm{d}t} = (-\Delta H)\left(-\frac{\mathrm{d}W}{\mathrm{d}t}\right) + \left(\frac{kA}{\delta}\right)(T_{\text{ana}} - T) \tag{10}$$

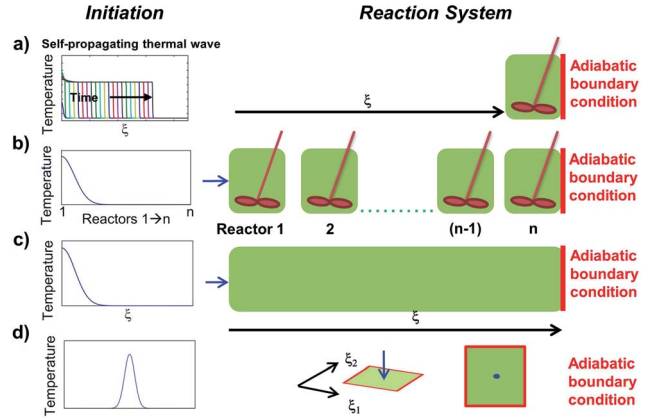

Fig. 1 Schematic of various reactor configurations used to illustrate superadiabaticity. (a) A batch reactor with adiabatic boundary, receiving heat input from a 1D self-propagating reaction wave. (b) Multiple batch reactors in series used to simulate a self-propagating reaction wave. Only the first batch reactor receives heat input. The last reactor has an adiabatic boundary and cannot exchange heat with the surroundings. (c) A 1D fuel layer with a Gaussian temperature input. (d) A 2D fuel layer, also with a Gaussian temperature input.

The heat transfer between the fuel layer and the incoming 1D reaction wave is accounted for by the term $\left(\frac{kA}{\delta}\right)(T_{\text{ana}} - T)$. The temperature profile of this self-propagating 1D reaction wave is given by T_{ana}, the thermal conductivity of the fuel is denoted by k, the surface area of heat exchange is A and δ is the thickness of a hypothetical membrane that limits the transfer. Thus (A/δ) corresponds to the main length scale for heat exchange. A simple first order reaction rate equation with Arrhenius rate constant is used in the fuel mass balance.

$$\frac{dW}{dt} = -k_0 W e^{-\frac{E_a}{RT}} \tag{11}$$

The corresponding non-dimensional forms of the equations are shown in eqn (12) and (13), using the same non-dimensional variables previously defined in eqn (3).

$$\frac{du}{d\tau} = \left(\frac{1}{\beta}\right)\left(-\frac{dw}{d\tau}\right) + (\gamma\beta)(u_{\text{ana}} - u) \tag{12}$$

$$\frac{dw}{d\tau} = -\beta w e^{-\frac{1}{u}} \tag{13}$$

where $u_{\text{ana}} = \dfrac{1/\beta}{(1 + Qe^{cQ(\xi - c\tau)})^{1/Q}}$

Here, the analytical temperature profile u_{ana} starts at a distance $\xi = \xi_0$ from the reactor and it affects the time it takes for the wave to reach the batch reactor. The value of ξ_0 is chosen to generate a defined region of zero reaction, $(\xi = \xi_0) > c\tau$. As time progresses, the self-propagating wave approaches the batch reactor and the (non-dimensional) temperature rises to $(1/\beta)$ *i.e.* $(u\beta) \sim 1$. The dimensionless heat transfer coefficient for the batch reactor is $\gamma = \dfrac{kA}{C_p\rho}\dfrac{1}{k_0}$. Both β and γ are dependent on the fuel and system properties respectively and are hence tunable. Changing the geometry of the reactor or fuel layer alters γ while the source of the fuel modifies β.

In our work, the set of coupled differential eqn (12) and (13) was numerically solved using MATLAB ordinary differential equation solver ode15s. We study the value of the normalized variable $(u\beta)$, which equals 1 for the adiabatic temperature. For a chosen value of β and γ, let us refer to the maximum temperature reached in the system as $u_{\max}$ and the time at which it occurs as $\tau_{\max}$. In Fig. 2, we plot color maps of $(u_{\max}\beta)$ for various values of β and γ.

As seen from Fig. 2, the numerical results show that superadiabatic temperatures up to values of $(u\beta) \sim 1.8$ exist for certain values of β and γ. Fig. 2b shows an output for $(u_{\max}\beta)$ reached by the fuel in the reactor zone for the values $(1 \le \beta \le 25)$ and $(0 \le \gamma \le 10^{-4})$ and $\xi_0 = 5000$. We chose values of β that are comparable to previously studied systems,[18,24] and we chose γ values to account for a wide range of system heat transfer properties. Superadiabaticity is observed to be dependent on both β and γ with β having a greater influence on existence of temperatures beyond the predicted $(u\beta) = 1$. Interaction between factors such as the energy of activation, heat of reaction, specific heat capacity of fuel and the heat loss coefficient determines whether the fuel layer demonstrates superadiabaticity under these conditions. As seen from Fig. 2, fuels with β between values of 5 to 15 have the potential to exhibit superadiabatic temperatures. As the value of γ increases, the

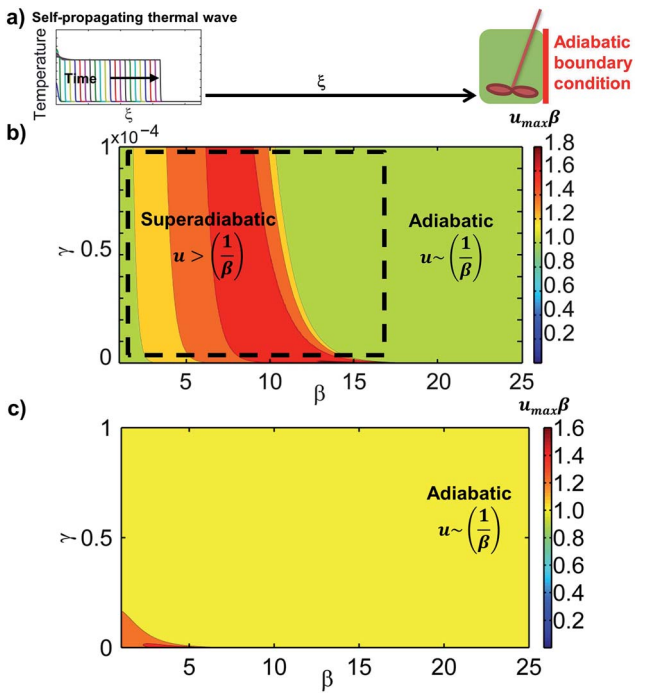

Fig. 2 (a) Schematic showing a batch reactor subjected to a 1D self-propagating reaction wave input. (b) For a single batch reactor, contour plot for $(u_{\max})\beta$ as a function of $1 \le \beta \le 25$ with a step size of 0.1 and $0 \le \gamma \le 10^{-4}$ with a step size of 10^{-7}. The area included in the dashed box shows region predicted to show superadiabaticity. (c) Contour plot for $(u_{\max})\beta$ for extended values of $0 \le \gamma \le 1$ with a step size of 10^{-4}.

rate at which the fuel loses heat increases and accordingly for high enough values of γ, no value of β can show superadiabatic temperature rise. If we extend the analysis for a less fine step size in γ but for values of γ up to 1, superadiabaticity ceases to exist for any value of β.

We note that the problem addressed in this work is one of closed reactant mass. The reactant mass and heat transfer rate cannot be adjusted independently. This closed mass condition is the case considered by Zeldovich and Frank-Kamenetskii and Mercer *et al.*,[16,23] and corresponds to the physical systems of solid phase inorganic synthesis, thermopower wave generation, and combustion synthesis. A trivial superadiabatic result arises if one allows reactant injection at regular intervals along the length of a propagating wave, but the result is a temperature that increases linearly and without bound along the length, leading to an unphysical system.

An order of magnitude analysis was performed on the governing heat balance equation in order to obtain an estimate of the bounds on the value of superadiabaticity. Assuming a continuous temperature profile, the temperature profile undergoes a maximum at the point of superadiabaticity. Thus at temperature u_{max}, as shown in Fig. 3, the first order derivative of temperature u with respect to time τ should be equal to zero.

$$\frac{du}{d\tau} = \left(\frac{1}{\beta}\right)\left(-\frac{dw}{d\tau}\right) + (\gamma\beta)(u_{ana} - u)$$

$$0 = \left(\frac{1}{\beta}\right)\left(-\frac{dw}{d\tau}\right) + (\gamma\beta)(u_{ana} - u) \quad (14)$$

$$\therefore \left(\frac{1}{\beta}\right)\left(\frac{dw}{d\tau}\right) = (\gamma\beta)(u_{ana} - u_{max})$$

Using substitution from eqn (13), we get:

$$\therefore -we^{-\frac{1}{u_{max}}} = (\gamma\beta)(u_{ana} - u_{max})$$

If $we^{-\frac{1}{u_{max}}} = 0$, there is no superadiabaticity. Thus, theoretically, the superadiabatic temperature is only attained at a non-zero fuel concentration.

$$u_{max} = u_{ana} + \frac{we^{-\frac{1}{u_{max}}}}{\gamma\beta} \quad (15)$$

Eqn (15) is an implicit equation for u_{max}. The 2nd term in eqn (15) accounts for heat generation within the reactor zone, and constants γ and β are critical to determine u_{max}. Eqn (15) allows one to evaluate the maximum possible value of superadiabaticity that can be theoretically obtained for a chosen system.

To validate our results from Fig. 2, we solve eqn (15) for w by choosing $\gamma = 10^{-5}$ and using corresponding numerical values for $u_{max}\beta$ from Fig. 2. In order to obtain bounds on the maximum value possible for u_{max}, we use maximum possible value of $u_{ana} = 1/\beta$. As can be seen from Fig. 4, systems showing superadiabatic temperatures show such temperatures for low values of w. Thus, by calculation using eqn (15), we show physically possible values of fuel concentrations at which systems might show superadiabatic temperature.

3.2. Superadiabatic temperature rise in a system of multiple batch reactors in series

We now study another system capable of superadiabatic behavior: a system of batch reactors in series. This system creates a fuel reaction and temperature profile effect similar to that observed in propagation of a reaction wave through a single continuous fuel domain. As can be seen from Fig. 1b, heat provided to the first reactor initiates an exothermic reaction, releasing heat which propagates to the next reactor. An adiabatic boundary condition imposed at the last reactor has the potential to concentrate the resulting reaction wave to temperatures exceeding the adiabatic limit. The system of non-dimensional equations for reactor n at time point i is given by:

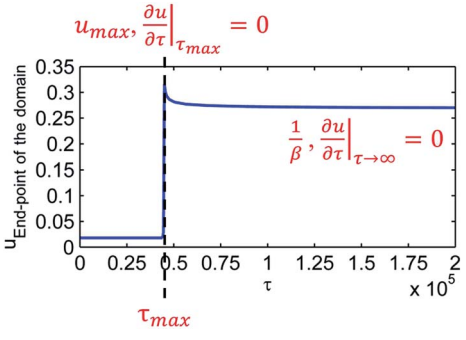

Fig. 3 Calculated temperature profile at the end-point of the reaction domain as a function of time, showing superadiabatic temperature u_{max}. According to the principles of derivatives, at the point of maxima, the first order derivative of temperature with respect to time will be zero.

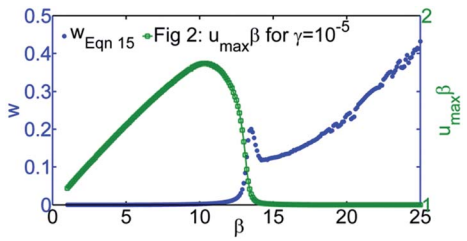

Fig. 4 w as a function of $1 \leq \beta \leq 25$ with a step size of 0.1 calculated using eqn (15) with $\gamma = 10^{-5}$, $u_{ana} = 1/\beta$ and corresponding numerical values of ($u_{max}\beta$) from Fig. 2. On the right hand side y-axis is the numerical data extracted from Fig. 2 for ($u_{max}\beta$) values corresponding to $\gamma = 10^{-5}$. This is for the case of a batch reactor subjected to a 1D self-propagating reaction wave input. We see that reactors which show superadiabatic temperature do so for $w \sim 0$. For systems showing maximum temperature of adiabatic temperature rise, they do so before complete conversion.

$$\left(\frac{du_{n,i}}{d\tau_i}\right) = \gamma_n(u_{n-1,i} - 2u_{n,i} + u_{n+1,i}) + \left(w_{n,i}e^{-\frac{1}{u_{n,i}}}\right) \quad (16)$$

$$\frac{dw_{n,i}}{d\tau_i} = -\beta w_{n,i}e^{-\frac{1}{u_{n,i}}} \quad (17)$$

where

$$\gamma_n = \frac{hA_nE_a}{k_0R(-\Delta H)C_{ref}}. \quad (18)$$

In eqn (16), the left hand side term corresponds to changes in the temperature of the n^{th} reactor with respect to time. The two terms on the right hand side correspond to heat exchange with the reactor that lies before and after the n^{th} reactor and the heat released because of reaction of the fuel in the n^{th} reactor. γ_n again stands for a non-dimensional heat transfer term that accounts for heat exchange between reactor n and the adjacent reactors $n - 1$ and $n + 1$. In eqn (18), h is the heat transfer coefficient governing exchange of heat across reactors over the shared surface area A_n and containing C_{ref} amount of fuel.

This coupled system of equations was solved using ode solver ode15s in MATLAB. A system of 50 equal-sized reactors ($n = 50$) was solved for a common heat transfer rate corresponding to $\gamma_n = 10^{-5}$. A non-zero input temperature $u_0 = 0.075$ was used to start the reaction in the first reactor. The output temperatures of each of the reactors were analyzed with respect to time. We note that the temperature profile of the reactors in series is approximately described by the continuous wave solution derived previously.[18] As anticipated, this system also demonstrates superadiabatic temperature rise where $(u\beta) > 1$. Fig. 5b shows the temperature profile in each of the entire system of reactors, just after the last reactor has reached complete conversion. As can be seen, all the reactors except the last one are at the adiabatic temperature rise *i.e.* $(u\beta = 1)$. However, the last reactor, which cannot lose heat in any way except *via* reflection to the penultimate reactor, shows superadiabatic temperature. In Fig. 5c, we plot the normalized temperature $(u\beta)$ as a function of the similarity variable $\eta = \xi - c\tau$, which captures the effect of wave propagation with distance travelled with respect to time. We compare the temperature profile of any two reactors, say reactor 25 and 35, to that of the 1D self-propagating reaction wave as obtained by using the analytical expression in eqn (7). As can be deduced from the figure, because of the nature of this numerical simulation, each of the reactors exhibits a superadiabatic temperature during the course of its reaction. Thus, any such fuel system with adiabatic boundaries exhibits superadiabatic temperature when nearing the end of its reaction.

In this system, the temperature of the reactor spikes to superadiabatic temperature once the temperature wavefront reaches an adiabatic boundary. The concept of superadiabaticity arises because of unequal time scales for heat exchange. While heat is given out by the reaction with the representative time scale of $\frac{1}{k_0}$, the heat is lost by the system by representative conductive heat loss governed by the time scale $\left[\left(\frac{A}{\delta}\right)^2 \Big/ \frac{k}{\rho C_p}\right]$. An imbalance between these time scales leads to a sudden accumulation of heat in the system leading to superadiabatic temperatures. According to Fourier's law, we expect such a superadiabatic system to start losing heat backwards into the system.

3.3. Superadiabacity from reaction waves over continuous reaction domains

Over a continuous reaction domain, superadiabacity can be observed when the resulting reaction wave impinges upon an adiabatic boundary condition. Fig. 6a shows a schematic of a 1D fuel layer along the dimension ξ. The coupled partial differential eqn (4) and (5) were solved using COMSOL. The simulation was carried out to study a non-dimensional domain 7000 units long and for $\beta = 4$. The total time of the simulation was chosen

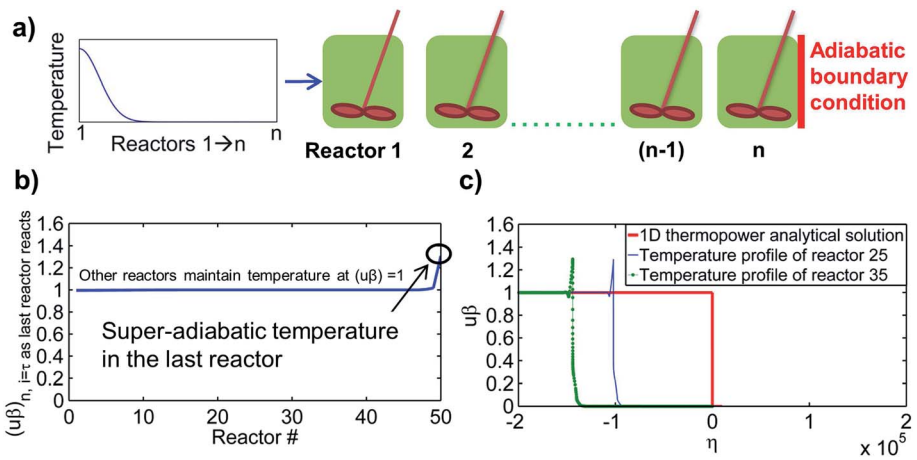

Fig. 5 (a) Schematic to study superadiabaticity in a system of multiple batch reactors in series, with the first reactor receiving input heat. (b) Temperature $(u\beta)$ at the time point just after the last reactor reacts completely. As seen from the figure, the last reactor shows elevated superadiabatic temperature. (c) Comparing temperature $(u\beta)$ for reactors 25 and 35 (of a total 50 reactors), with the analytical solution for a 1D self-propagating reaction wave as a function of similarity variable $\eta(\xi,\tau)$.

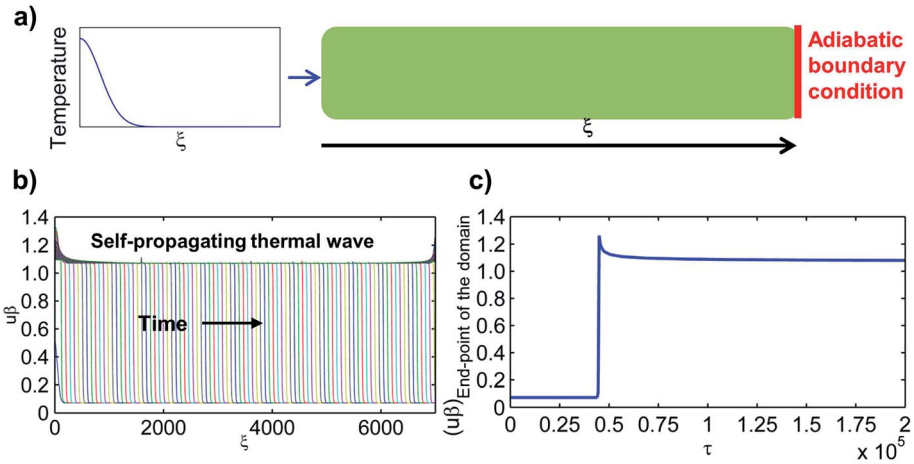

Fig. 6 (a) Schematic of a system of a 1D fuel layer with a Gaussian heat input. (b) Plots for temperature along the length of the 1D domain. Each curve corresponds to the temperature profile at one time point. Output is obtained from COMSOL simulation for conditions $\beta = 4$ for $\xi = (0 : 2 : 7000)$ and $\tau = (0 : 500 : 200\,000)$. (c) Temperature at the last boundary point of the 1D domain plotted as a function of time. The peak in temperature corresponds to a superadiabatic temperature.

such that the fuel reaction would reach completion. Similar to the previous[18,24] analyses, we observe steady state wave propagation; however, in this case we examine the limit of the wave impingement upon the adiabatic boundary. Fig. 6b plots the temperature of the wavefront as a function of distance, for each time point where calculations were performed. Each colored trace corresponds to the snapshot of temperature along the domain length at different reaction times. As the reaction proceeds, the temperature behind the wavefront reaches a value of $(1/\beta)$ as expected. The simulation was conducted at $\beta = 4$ and hence we observe a steady state (non-dimensional) temperature of about $u = 0.25$. As the wavefront approaches the adiabatic boundary, the temperature becomes superadiabatic. Over time, this temperature peak loses its heat back into the system. In Fig. 6c, we plot the temperature at the domain boundary with respect to time τ. This plot clearly shows superadiabaticity with maximum temperature value almost up to $(u\beta) \sim 1.26$ as against the steady state propagation temperature of $(u\beta) \sim 1.07$.

3.4. Superadiabacity in 2D reaction systems

We next study the concept of bounded self-propagating waves in two-dimensional (2D) systems. While the previously discussed work by Mercer,[21–23] Weber,[20] and others show the presence of 2D self-propagating waves, we also confirm it by using a different and simplified system of equations. For an isotropic system with uniform physical properties in all directions, a 2D Cartesian coordinate system is mathematically equivalent to a 1D radial system of equations, and is computationally less expensive than solving the 2D Cartesian equations. Here, we examine the radial 1D system shown in Fig. 7a, where an adiabatic boundary is established at the circumference at $r = r_{max}$. The governing set of non-dimensional 1D radial coordinate system equations for a solid fuel reaction are given by eqn (19) and (20).

$$\frac{\partial u}{\partial \tau} = \frac{1}{r}\left[\frac{\partial}{\partial r}\left(r\frac{\partial u}{\partial r}\right)\right] + e^{-1/u}w \tag{19}$$

$$\frac{dw}{d\tau} = -\beta w e^{-1/u} \tag{20}$$

The non-dimensional radial coordinate is represented by r. A numerical solution for the above set of equations was obtained using COMSOL. Again, the simulation was carried out to study a non-dimensional domain of size ($r_{max} = 7000$ units) for $\beta = 4$, and the total time of the simulation was chosen such that the fuel reaction would reach completion. A Gaussian temperature peak was used for initiating the reaction:

$$u_0 = g e^{-\frac{r^2}{w_d}} + u_{ambient} \tag{21}$$

In eqn (21), g corresponds to the maximum intensity of the Gaussian peak (*i.e.* the maximum input temperature) and w_d corresponds to the width of the peak. The numerical results were analyzed to study the steady state propagation of the wave by considering the adiabatic boundary condition. As can be seen in Fig. 7, the results show the existence of a self-propagating reaction wave.

Fig. 7b is similar to Fig. 6b. Both these plots demonstrate self-propagating waves along a distance coordinate. As in the case of the 1D (Cartesian) thermal wave, the maximum temperature reached behind a steady-state 1D radial thermal wave was found to be proportional to $(1/\beta)$. This feature was confirmed for a range of β values from 3 to 10, as shown in Fig. 7c.

After confirming the existence of these waves, we moved onto computationally expensive 2D Cartesian simulations for a physically 2D system, where ξ_1 and ξ_2 are the two perpendicular non-dimensional distance coordinates.

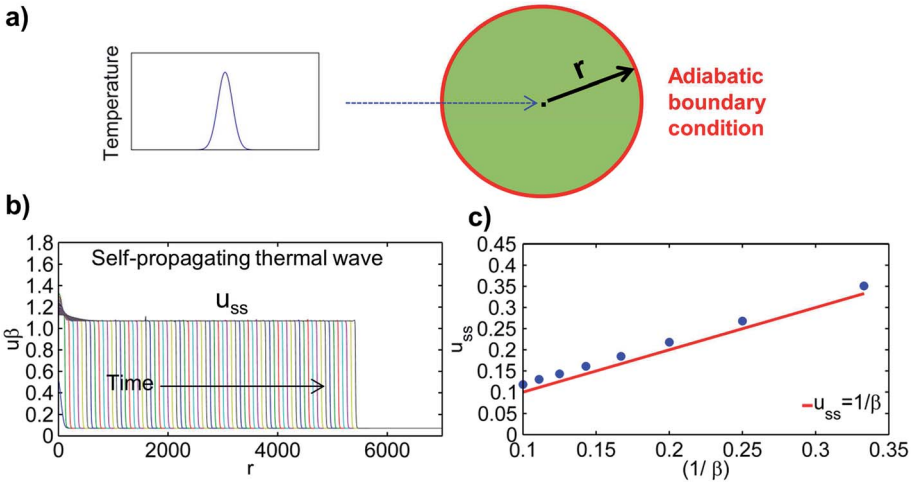

Fig. 7 (a) Schematic to study self-propagating reaction waves in a 1D radial system of a layer of fuel with a Gaussian heat input. (b) Output from a 1D radial reaction wave simulation. Simulation parameters used were: $\beta = 4$ for $r = (0 : 2 : 7000)$ and $\tau = (0 : 500 : 200\,000)$. u_0 was set using $g = 0.1$ and $w_d = 5000$. The figure plots u *vs.* r for multiple time points. (c) Non-dimensional steady state propagation temperature u_{ss} plotted with respect to $(1/\beta)$. As expected, we observe that $u_{ss} \sim (1/\beta)$ as the 2D wave becomes a 1D reaction front. The upshift in the points is because of the initiation condition.

$$\frac{\partial u}{\partial \tau} = \frac{\partial^2 u}{\partial {\xi_1}^2} + \frac{\partial^2 u}{\partial {\xi_2}^2} + w e^{-\frac{1}{u}} \tag{22}$$

$$\frac{dw}{d\tau} = -\beta w e^{-\frac{1}{u}} \tag{23}$$

To study the 2D Cartesian system, the initial Gaussian peak condition was also modified to a 2D Cartesian form:

$$u_0 = g e^{-\frac{{\xi_1}^2 + {\xi_2}^2}{w_d}} + u_{\text{ambient}} \tag{24}$$

Simulations were carried out with adiabatic boundary condition at all the boundaries.

$$\left.\frac{\partial u}{\partial \xi_1}\right|_{\text{boundary}} = \left.\frac{\partial u}{\partial \xi_2}\right|_{\text{boundary}} = 0 \tag{25}$$

Fig. 1d shows schematic of a square fuel layer receiving temperature input in the form of a Gaussian curve. Simulations for such a square geometry re-confirmed existence of self-propagating two dimensional reaction waves. The temperature behind the wavefront was found to be proportional to $(1/\beta)$. This type of system also showed superadiabaticity where a sudden rise in temperature was observed once the wave reached the boundary, because there is no 'forward' path to lose heat generated by the exothermic reaction of the fuel. This leads to the heat being confined to the region near the boundary, and leads to increased temperature. Experimentally, while it is not possible to obtain perfectly adiabatic conditions, it is possible to reduce heat loss by tuning experimental conditions such as carrying out the reaction in vacuum to reduce convective losses or performing the reaction in an enclosed chamber with walls having low thermal conductivity.

For the purpose of confirming superadiabaticity in additional 2D systems, a fuel layer in the shape of an equilateral triangle was selected to explore the effect of geometry, as shown in Fig. 8. The reaction is initiated with heat along the bottom edge of the triangle, with the form given below:

$$u_0 = g e^{-\frac{{\xi_2}^2}{w_d}} + u_{\text{ambient}} \tag{26}$$

Fig. 8a–d show color maps of the temperature across the triangular fuel layer as the reaction wave propagates. Here, the system exhibits a superadiabatic temperature rise at $\tau = 360$. Fig. 8e plots temperature $(u\beta)$ at the two vertices of an equilateral triangle: vertex 1 is at one of the corners along the edge where the reaction is initiated, and vertex 2 is at the corner opposite the initiation edge. The temperature peak shown by vertex 2 demonstrates superadiabaticity.

This result opens up new avenues for research to study the bounds of superadiabaticity in 2D domains. Preliminary work on 2D numerical COMSOL simulations for different shapes for 2D fuel conduits show interesting temperature profiles, in that edges or regions of adiabatic boundary show varying degrees of superadiabaticity. Future work in this area will focus on studying these waves and heat reflection in such systems in more detail. Wave-guides can be designed to maximize the temperature reached thus allowing for improved ways to harvest chemical energy in the form of heat.

4. Applications of superadiabaticity

Superadiabaticity allows one to extract higher temperatures from the same quantity of fuel by manipulating reaction conditions. We propose that this has the potential to offer advantages for converting chemical energy to electrical energy. In systems that use a thermal conduit to aid the self-propagation of fuel reactions, we can choose thermoelectric materials as the thermal conduit. Therefore, higher temperatures will give rise to

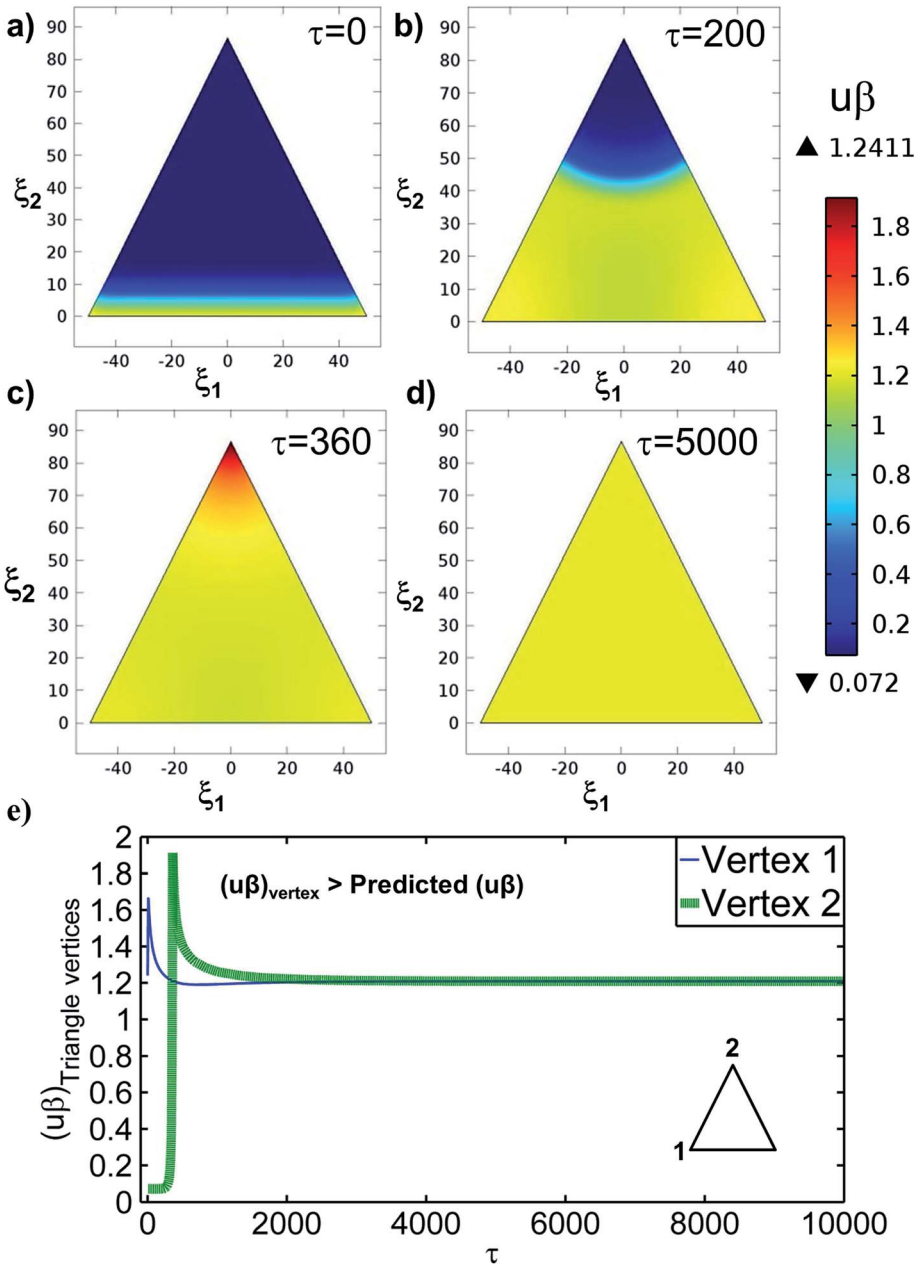

Fig. 8 Output from 2D Cartesian reaction wave simulation for an equilateral triangle geometry with line initiation ($g = 0.25$, $w_d = 50$, $u_{ambient} = 0.018$), at $\beta = 4$. (a–d) These sections show a color-maps of temperature across the surface of the 2D fuel layer at various time points of $\tau = 0$, $\tau = 200$, $\tau = 360$ and $\tau = 5000$. Superadiabatic temperature can be seen at $\tau = 360$ when temperature at the top vertex of the triangle shows a maximum. (e) The figure shows presence of superadiabaticity at the top vertex of the triangle away from the line of initiation with temperature as high as $(u\beta) \sim 1.9$. Peak in temperature at vertex 1 corresponds to the initiation input heat.

an increased temperature gradient and thus increased electrical output. It might also give an added advantage when using materials like annealed ZnO thin films, annealed Ga-doped ZnO thin films or Ga-doped ZnO alloy that exhibit Seebeck coefficients that increase with increasing temperature of operation.[5,9]

4.1. Modified thermophotovoltaics

A conventional thermophotovoltaic consists of a reaction chamber that heats an emitter, which in turn gives out radiation that is absorbed by an absorber or a photovoltaic (PV) and then converted to an electrical output.[11,12] Often there is an additional filter included to moderate the wavelength of the light incident on the photovoltaic and thus increase the efficiency of operation.[11,12] To exploit superadiabaticity, we envision a modified thermophotovoltaic wave system where our reaction chamber and the emitter is the reacting fuel layer.

Fig. 9a shows the schematic for a modified thermophotovoltaic. The device operation consists of three steps: (1) fuel loading, possibly onto a thermal conduit, (2) chemical reaction and (3) harvesting the radiation using a PV. Thus, overall

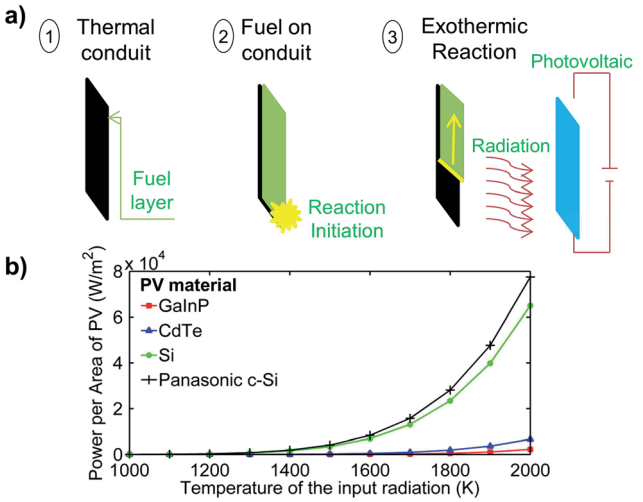

Fig. 9 (a) Schematic explaining the concept of modified thermo-photovoltaic wave system. First step involves depositing a fuel layer, possibly atop a thermal conduit. Fuel reaction is then initiated by means of an external source of ignition. As the reaction wave propagates, radiation is emitted by the reaction wavefront. This radiation is harvested by a photovoltaic. (b) Comparing the power output per unit area from modified thermophotovoltaic for different materials for PV, studied as a function of temperature of input radiation.

efficiency of this modified thermophotovoltaic system depends on two factors: (1) the temperature of the reaction, which affects the radiation emitted by the reaction, which then acts as the input to the photovoltaic, and (2) the efficiency of the photovoltaic to convert the input radiation into electricity. The second factor is dependent on the rapidly developing field of photovoltaics.[33] A device efficiency as high as 37.9% has been reported for an InGaP/GaAs/InGaAs solar cell fabricated by Sharp.[33] We assume the radiation emitted by the fuel reaction is governed by Planck's law of blackbody radiation, so that the higher the temperature at which the radiation is emitted, the higher the intensity of light radiated at each wavelength. Also, as the temperature at which the radiation is emitted increases, the wavelength at the peak of the intensity spectrum shifts towards the visible region. Currently, the best photovoltaics being developed are designed to harvest the radiation of the visible solar spectrum. Higher reaction temperatures disproportionately shift the radiation to wavelengths that are more efficient for visible photovoltaics to harvest. Thus, by appropriate tuning of the system properties and proper fuel selection, we can obtain superadiabatic temperatures, which will improve the overall operation efficiency of the modified thermophotovoltaic system. We have performed calculations that show that the overall energy efficiency of this system increases as the temperature of the input radiation increases. The PV materials we studied were based on GaInP,[34] CdTe,[35] Si,[36] and a large area Si cell from Panasonic (*i.e.* Panasonic c-Si cell),[33] in increasing order of their efficiency.

The radiation output profile emitted by the fuel layer $B_\lambda(T)$ is calculated using Planck's law. It is a function of absolute temperature T and wavelength λ. Other parameters used are speed of light c, Boltzmann constant k_B and Planck constant h.

$$B_\lambda(T) = \frac{2hc^2}{\lambda^5}\frac{1}{e^{\frac{hc}{\lambda k_B T}} - 1} \quad (27)$$

At the same temperature, the heat losses in the form of conduction, convection and radiation are calculated. Conductive heat loss L_d is a function of the mass of the fuel or conduit layer (if any) m_f, specific heat capacity $C_{p,f}$, duration of the fuel reaction t_{rxn} and the area available for heat exchange A.

$$L_d(T) = \frac{m_f C_{p,f}(T - T_{amb})}{t_{rxn} A} \quad (28)$$

Convective heat loss L_v is a function of mass of the (gaseous) products m_p, specific heat capacity $C_{p,p}$, duration of the fuel reaction t_{rxn} and the area available for heat exchange A.

$$L_v(T) = \frac{m_p C_{p,p}(T - T_{amb})}{t_{rxn} A} \quad (29)$$

Radiative heat loss L_r is given by the Stefan–Boltzmann law, where σ is the Stefan–Boltzmann constant:

$$L_r(T) = \sigma(T^4 - T_{amb}{}^4) \quad (30)$$

The sum of these three heat fluxes (unit of power per unit area) is the total input in the system consisting of the photovoltaic and the fuel layer, although only the radiative energy will be used by the PV to generate electrical energy. In order to calculate the output of electrical energy from the system, the input radiation curve $B_\lambda(T)$ is then super-imposed over the external quantum efficiency (EQE) curve for the photovoltaic cell being studied. The EQE curve of a PV cell measures the efficiency with which the cell can convert the incident photons (*i.e.* absorbed radiation) into electricity. In order to obtain the total output from the cell, this value of product of EQE with the input radiation spectrum is integrated over the entire range of wavelength to obtain the net power output.

$$L_{out}(T) = \int B_\lambda(T) \times \mathrm{EQE}(\lambda)\mathrm{d}\lambda \quad (31)$$

The overall efficiency of the system E is calculated as a ratio of the net electrical power output upon the total input to the system.

$$E(T) = \frac{L_{out}(T)}{L_d(T) + L_v(T) + L_r(T)} \quad (32)$$

From our calculations, as seen in Fig. 9b, an increase in temperature gives an improved output in power obtained per unit area of the photovoltaic cell. Also, photovoltaic devices of materials such as Si which have a higher overall efficiency can make better use of this improved input leading to a much higher output at higher temperatures, especially when compared to lower overall efficiency photovoltaic cells such as GaInP and CdTe. Improvement in temperature of the input radiation from 1000 K to 2000 K leads to an almost 4000-fold increase in output power per unit area.

For carrying out calculations for efficiency of thermophotovoltaics at different temperatures of input radiation, as shown in eqn (32), the temperature dependent output from the thermophotovoltaic system is calculated using the Planck's law and the photovoltaic cell's EQE curve (Fig. 9b). Calculations pertaining to the input to the system are based off of a preliminary experiment carried out in our lab where about a 4 second long reaction wave of 60 mg of nitrocellulose was launched over the thermal conduit of 44 mg of aluminum over a surface area of about 10 cm^2. Since we want to perform input calculations only as a function of temperature, we calculate the heat input not *via* the fuel energy content but by calculating the total power per unit area from all three modes of heat transfer; radiation (eqn (30)), convection (eqn (29)) and conduction (eqn (28)). In evaluating the convective component of the heat transfer rate per unit area, we assume ideal gas properties for the specific heat capacity of gaseous products formed and about 11 moles of gaseous products formed per mole of fuel reacted with the total fuel content of about 0.24 moles (where molar values are based on the case of nitrocellulose reaction).

At the input radiation temperature of 2000 K, the overall efficiency of operation of such modified thermophotovoltaics setup was calculated to be about 8.2% for the Panasonic c-Si cell, about 6.9% for the conventional Si cell, about 0.7% for the CdTe cell and just about 0.24% for the GaInP cell.

Thus, when superadiabaticity is used in combination with high efficiency photovoltaic cells such as the Si-based photovoltaic cells, it is possible to obtain electrical output with almost 8% overall efficiency. These values are comparable to the demonstrated efficiencies in the range of 0.6% to 11% for prototypes of conventional thermophotovoltaic systems.[12] Traditional thermophotovoltaic reaction chambers use fossil fuels to reach high temperatures.[11,12] With this new thermophotovoltaic wave setup, we can use novel fuels such as nitrocellulose to reach comparably high temperatures by superadiabaticity. Moreover, this helps us obtain higher temperatures without the disadvantage of additional nitrous oxide production at higher temperature combustion reactions.[11,12] Also, as mentioned before, the preliminary calculations shown above do not account for using a filter for wavelength selection and re-using unused photons to heat the thermal conduit.[12] Thus, there is the possibility for further improvement in operation of the modified thermophotovoltaic wave system.

5. Conclusion

After analytical and numerical analysis of heat transfer in various systems of self-propagating reaction waves such as a self-propagating 1D reaction wave, multiple batch reactors in series and a self-propagating 2D reaction wave, we show the occurrence of superadiabatic temperatures in the presence of adiabatic boundaries. Numerical analysis of various systems of governing heat and mass balance equations was performed using MATLAB and COMSOL. Analytical bounds for superadiabaticity were obtained by simplifying the governing non-linear differential equations. For all these cases, when a reaction wave impacts on an adiabatic boundary, the interplay of the heat retaining capacity of the fuel and the heat transfer coefficient within the system leads to superadiabaticity. Our simulations for these cases predict temperatures up to 1.8 times higher than that expected by the adiabatic temperature rise. This result opens up avenues for applications in areas such as thermopower waves, high temperature self-propagating synthesis, thermoelectrics and modified thermophotovoltaics. Further research is needed to take advantage of superadiabaticity to more efficiently convert chemical energy to usable electrical energy.

References

1 L. D. Schmidt, *Engineering of Chemical Reactions*, Oxford University Press, 2nd edn, 2005.
2 S. Hada and B. K. Harrison, *J. Loss Prev. Process Ind.*, 2007, **20**, 151–157.
3 S. McAllister, J.-Y. Chen and A. C. Fernandez-Pello, *Fundamentals of combustion processes*, [electronic resource], Springer, New York, 2011.
4 A. G. Merzhanov, *J. Mater. Chem.*, 2004, **14**, 1779–1786.
5 J. M. Smith, H. C. Van Ness and M. M. Abbott, *Introduction to Chemical Engineering Thermodynamics*, McGraw Hill Higher Education, 6th edn, 2003.
6 F. J. DiSalvo, *Science*, 1999, **285**, 703–706.
7 G. J. Snyder and E. S. Toberer, *Nat. Mater.*, 2008, **7**, 105–114.
8 A. Bejan and A. D. Kraus, *Heat Transfer Handbook*, John Wiley & Sons, 2003.
9 J. H. V. Lienhard and J. H. I. V. Lienhard, *A Heat Transfer Textbook*, Dover Publications, 4th edn, 2011.
10 H. D. Baehr and K. Stephan, *Heat and Mass Transfer*, Springer Berlin Heidelberg, 3rd revised edn, 2011.
11 T. J. Coutts and M. C. Fitzgerald, *Sci. Am.*, 1998, **279**, 68–73.
12 M. Bosi, C. Ferrari, F. Melino, M. Pinelli, P. R. Spina and M. Venturini, 'Thermophotovoltaic generation: A state of the art review', *Proceedings of the 25th int conf on efficiency, cost, optimization, simulation and environmental impact of energy systems*, Perugia, Italy, 2012.
13 V. Rinnerbauer, S. Ndao, Y. X. Yeng, W. R. Chan, J. J. Senkevich, J. D. Joannopoulos, M. Soljacic and I. Celanovic, *Energy Environ. Sci.*, 2012, **5**, 8815–8823.
14 S. T. Aruna and A. S. Mukasyan, *Curr. Opin. Solid State Mater. Sci.*, 2008, **12**, 44–50.
15 W. Choi, S. Hong, J. T. Abrahamson, J.-H. Han, C. Song, N. Nair, S. Baik and M. S. Strano, *Nat. Mater.*, 2010, **9**, 423–429.
16 Y. B. Zeldovich and D. Frank-Kamenetskii, *Zh. Fiz. Khim.*, 1938, **12**, 100–105.
17 P. Gray and W. Kordylewski, *Proc. R. Soc. London, Ser. A*, 1985, **398**, 281–288.
18 J. T. Abrahamson and M. S. Strano, *J. Phys. Chem. Lett.*, 2010, **1**, 3514–3519.
19 J.-H. He, *Abstract and Applied Analysis*, 2012, **2012**, 130.
20 R. O. Weber, G. N. Mercer, H. S. Sidhu and B. F. Gray, *Proc. R. Soc. London, Ser. A*, 1997, **453**, 1105–1118.
21 G. N. Mercer and R. O. Weber, *Combust. Theory Modell.*, 1997, **1**, 157–165.
22 G. N. Mercer and R. O. Weber, *Proc. R. Soc. London, Ser. A*, 1995, **450**, 193–198.

23 G. N. Mercer, R. O. Weber and H. S. Sidhu, *Proc. R. Soc. London, Ser. A*, 1998, **454**, 2015–2022.
24 J. T. Abrahamson, W. Choi, N. S. Schonenbach, J. Park, J.-H. Han, M. P. Walsh, K. Kalantar-zadeh and M. S. Strano, *ACS Nano*, 2010, **5**, 367–375.
25 S. G. Mahajan, Q. H. Wang, M. S. Strano and J. T. Abrahamson, *AIChE J.*, 2013, **59**, 3333–3341.
26 J. T. Abrahamson, C. Song, J. H. Hu, J. M. Forman, S. G. Mahajan, N. Nair, W. Choi, E.-J. Lee and M. S. Strano, *Chem. Mater.*, 2011, **23**, 4557–4562.
27 J. T. Abrahamson, B. Sempere, M. P. Walsh, J. M. Forman, F. Şen, S. Şen, S. G. Mahajan, G. L. C. Paulus, Q. H. Wang, W. Choi and M. S. Strano, *ACS Nano*, 2013, **7**, 6533–6544.
28 S. Walia, R. Weber, S. Balendhran, D. Yao, J. T. Abrahamson, S. Zhuiykov, M. Bhaskaran, S. Sriram, M. S. Strano and K. Kalantar-zadeh, *Chem. Commun.*, 2012, **48**, 7462–7464.
29 S. Walia, R. Weber, K. Latham, P. Petersen, J. T. Abrahamson, M. S. Strano and K. Kalantar-zadeh, *Adv. Funct. Mater.*, 2011, **21**, 2072–2079.
30 S. Walia, R. Weber, S. Sriram, M. Bhaskaran, K. Latham, S. Zhuiykov and K. Kalantar-zadeh, *Energy Environ. Sci.*, 2011, **4**, 3558–3564.
31 S. Walia, S. Balendhran, P. Yi, D. Yao, S. Zhuiykov, M. Pannirselvam, R. Weber, M. S. Strano, M. Bhaskaran, S. Sriram and K. Kalantar-zadeh, *J. Phys. Chem. C*, 2013, **117**, 9137–9142.
32 S. Hong, W. Kim, S.-J. Jeon, S. C. Lim, H.-J. Lee, S. Hyun, Y. H. Lee and S. Baik, *J. Phys. Chem. C*, 2013, **117**, 913–917.
33 M. A. Green, K. Emery, Y. Hishikawa, W. Warta and E. D. Dunlop, *Progress in Photovoltaics: Research and Applications*, 2013, **21**, 827–837.
34 S. Lu, L. Ji, W. He, P. Dai, H. Yang, M. Arimochi, H. Yoshida, S. Uchida and M. Ikeda, *Nanoscale Res. Lett.*, 2011, **6**, 576.
35 M. Hädrich, H. Metzner, U. Reislöhner and C. Kraft, *Sol. Energy Mater. Sol. Cells*, 2011, **95**, 887–893.
36 Y. Xia, B. Liu, J. Liu, Z. Shen and C. Li, *Sol. Energy*, 2011, **85**, 1574–1578.